

Fabrication of Particles and Crystals of Poly(*p*-phenylene pyromelliteimide) and the Study on Crystal Structure

Kanji Wakabayashi,[†] Tetsuya Uchida,[‡] Shinichi Yamazaki,[†] Kunio Kimura,^{*,†} and Kaoru Shimamura[‡]

Graduate School of Environmental Science, Okayama University, 3-1-1 Tsushima-naka, Okayama 700-8530, Japan, and Graduate School of Natural Science and Technology, Okayama University, 3-1-1 Tsushima-naka, Okayama 700-8530, Japan

Received September 2, 2006; Revised Manuscript Received October 2, 2006

ABSTRACT: Morphologies of poly(*p*-phenylene pyromelliteimide) (PPPI) were investigated by using phase separation during polymerization of pyromellitic dianhydride (PMDA) and *p*-phenylene diamine (PPDA). Polymerizations were carried out at 330 °C for 6 h. PPDA was added to the solution of PMDA in an aromatic solvent at various temperatures after PMDA was entirely dissolved. The morphology of the precipitates was drastically changed with the temperature of PPDA addition (*Tad*). When *Tad* was 240 °C, the fine particles were formed through the formation of droplets via liquid–liquid phase separation. On the contrary, when *Tad* was higher than 280 °C, the mixture of lozenge-shaped crystals and starlike aggregates of needlelike crystals were formed by the crystallization of oligomers. *Tad* influenced the degree of imidization of oligomers, resulting in the variation in the morphology of PPPI. Crystal structure and molecular chain orientation of the lozenge-shaped crystals were also investigated by high-resolution transmission electron microscope.

1. Introduction

Nano- and micrometer scale polymer architectures have been receiving much attention to create new materials for supporting nanotechnology.^{1–4} A wide variety of polymer materials such as tubes, wires, and particles has been fabricated by self-assembling,⁵ nanoprocessing technology represented by electrospinning⁶ and so on. Aromatic rigid polymers have been expected as hopeful candidates for not only high-performance but also functional materials.⁷ Although academic demands in aromatic rigid polymers gradually enhance in these days, they usually exhibit neither solubility nor fusibility due to their rigidity, and this intractability makes them inaccessible to process by conventional procedures. A new procedure for the architecture of aromatic rigid polymers is eagerly required.

Recently, the authors studied the morphology control of poly(*p*-phenylene pyromelliteimide) (PPPI), which is the highest class of superengineering plastics,^{8–12} by using phase separation during solution polymerization. Lozenge-shaped crystals and fine particles of PPPI were prepared (Scheme 1) by the polymerization of pyromellitic dianhydride (PMDA) and *p*-phenylene diamine (PPDA) in poor solvents at high temperature.¹³ These morphologies were determined by the phase-separation mode of oligomers, that is, crystallization or liquid–liquid phase separation, and they were highly dependent on the polymerization conditions such as solvents, polymerization temperatures, and concentrations. The polymerizations were carried out by the addition of PPDA into the solution of PMDA, and it was found that the morphology of PPPI was drastically changed with the temperature of PPDA addition (*Tad*). However, the influence of *Tad* remained unclear.

This paper aims to clarify the influence of *Tad* on the morphology of PPPI and describe the structure of the obtained crystals.

2. Experimental Section

2.1. Materials. PMDA was purchased from Aldrich Co. Ltd. and purified by sublimation. PPDA was a gift of Taishin Kasei Kogyo Co. Ltd. and used as received. Therm S-1000 (TS10, a mixture of isomers of dibenzyltoluene) was purchased from Nippon Steel Chemical Co. Ltd. and purified by distillation under reduced pressure (165–170 °C/0.2 mmHg).

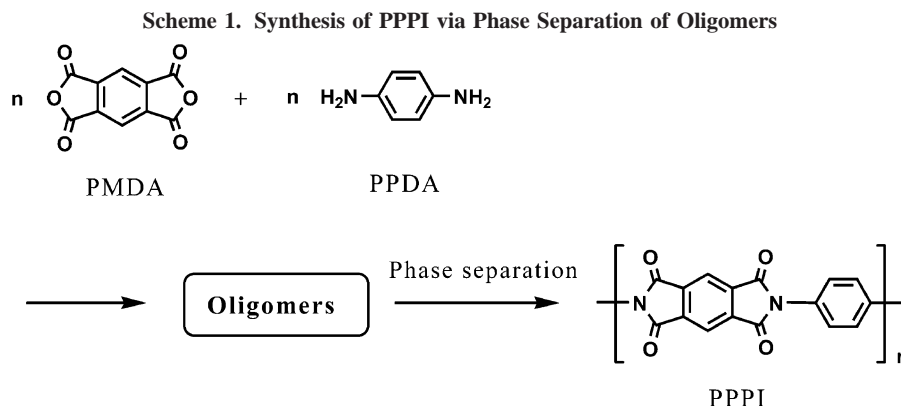
2.2. Measurement. Morphology of the products was observed on a Hitachi S-3500N scanning electron microscope (SEM) at 20 kV and a JEOL 2000EX transmission electron microscope (TEM) at 200 kV. The selected-area electron diffraction and dark-field image of the product were also taken on a TEM. Average shape parameters of the products were determined by taking the average of over 200 observation values. Infrared (IR) spectra were recorded on a JASCO FT/IR-410 spectrometer. Matrix-assisted laser desorption ionization time-of-flight mass spectrometry (MALDI-TOF MS) were performed on a Bruker Daltonics AutoFLEX MALDI-TOF MS system operating with a 337-nm N₂ laser. Spectra were obtained in the linear positive mode with an accelerating potential of 20 kV. Mass calibration was performed with angiotensin I (MW 1296.69) and insulin B (MW 3496.96) from a Sequazyme peptide mass standard kit. The samples were then prepared by the evaporation-grinding method and ran in 3-aminoquinoline as a matrix doped with potassium trifluoroacetate salt according to the reported procedure.¹⁴ Density of the products were measured by the flotation method with toluene and bromoform at 25 °C. The degree of imidization (DI) was calculated from the intensity ratio of the imide band at 1380 cm⁻¹ (C–N stretching) to the reference band at 1500 cm⁻¹ (C=C stretching of benzene ring) in the IR spectra according to the reported procedure.¹⁵

2.3. Polymer Preparation. PMDA (0.075 mg, 0.34 mmol) and 20 mL of TS10 were placed into a cylindrical flask equipped with a gas inlet tube, and the reaction mixture was heated to 330 °C with stirring in N₂. After PMDA was entirely dissolved on heating,

* To whom correspondence should be addressed (tel and fax: +81-86-251-8902, e-mail: polykim@cc.okayama-u.ac.jp).

[†] Graduate School of Environmental Science.

[‡] Graduate School of Natural Science and Technology.



PPDA (0.037 mg, 0.34 mmol) was added at given temperatures such as 240, 280, and 330 °C into the solution under stirring. The stirring was stopped within 5 s, and then the polymerization was carried out at 330 °C for 6 h with no stirring. The solution became immediately turbid due to the precipitation of oligomers, and the orange precipitates were generated in the solution. After 6 h, the precipitated products were collected by vacuum filtration at 330 °C, washed with *n*-hexane and acetone, and then dried at 25 °C for 12 h. Oligomers left in the solution at 330 °C were recovered by filtration after the precipitation by pouring the filtrate into *n*-hexane.

3. Results and Discussion

3.1. Influence of *Tad* on Morphology. The morphology of the products is drastically changed with *Tad* as previously reported.¹³ When *Tad* was 240 °C, the particles were formed through the liquid–liquid phase separation. On the other hand, when *Tad* was higher than 280 °C, mixtures of starlike aggregates of needlelike crystals (SA) and lozenge-shaped crystals were formed by the crystallization.

To understand the influence of *Tad* on the morphology, changes in the yield, average diameter and number of the

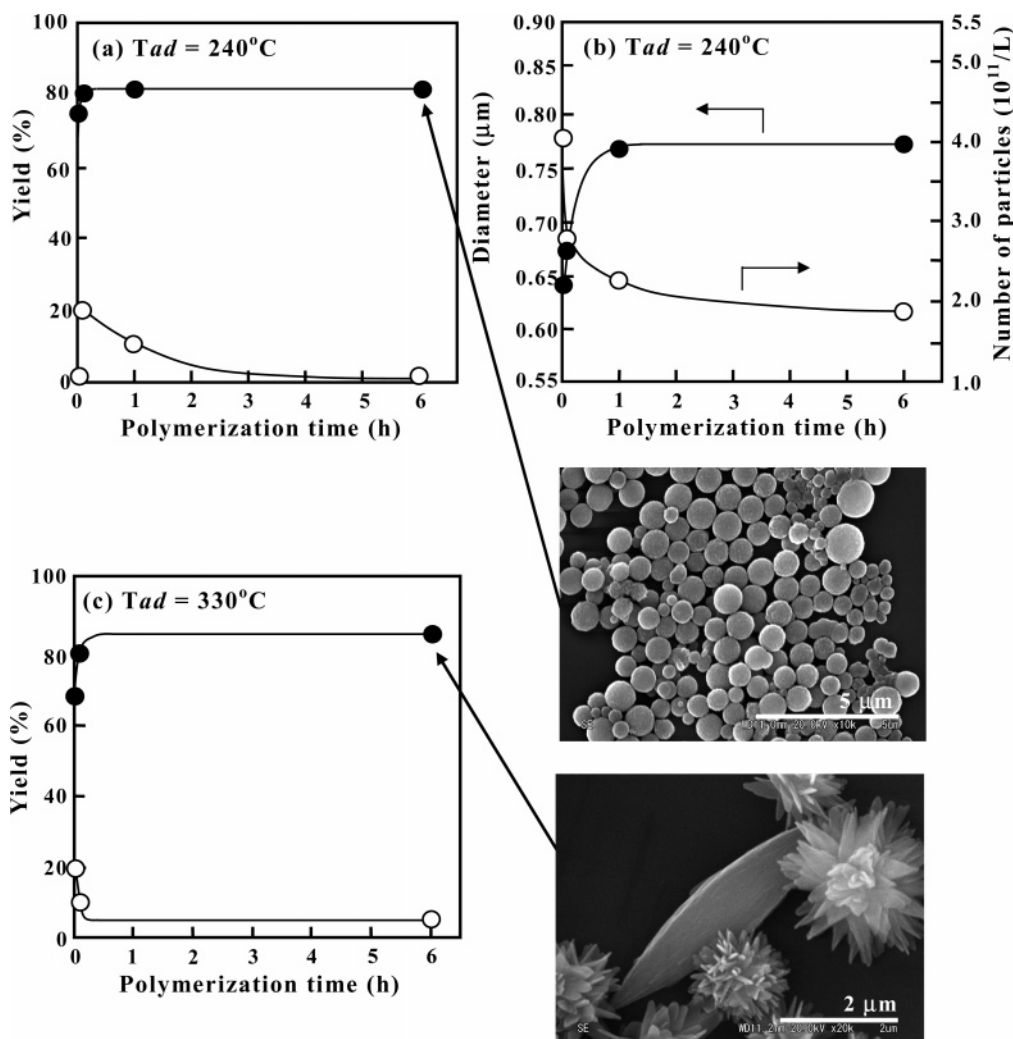


Figure 1. Plots of (a) yield of particles (●) and recovery yield of dissolved oligomers (○), and (b) the average diameter (●) and number of particles (○) prepared at *Tad* of 240 °C as a function of polymerization time. Plots of (c) yield of crystals (●) and recovery yield of dissolved oligomers (○) prepared at *Tad* of 330 °C as also a function of polymerization time. *Tad* stands for the temperature of PPDA addition.

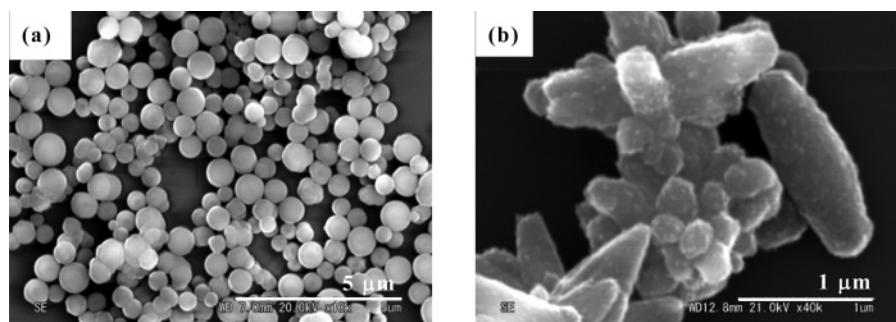


Figure 2. Initial morphological features of (a) particles and (b) lozenge-shaped crystals and SAs prepared for 30 s.

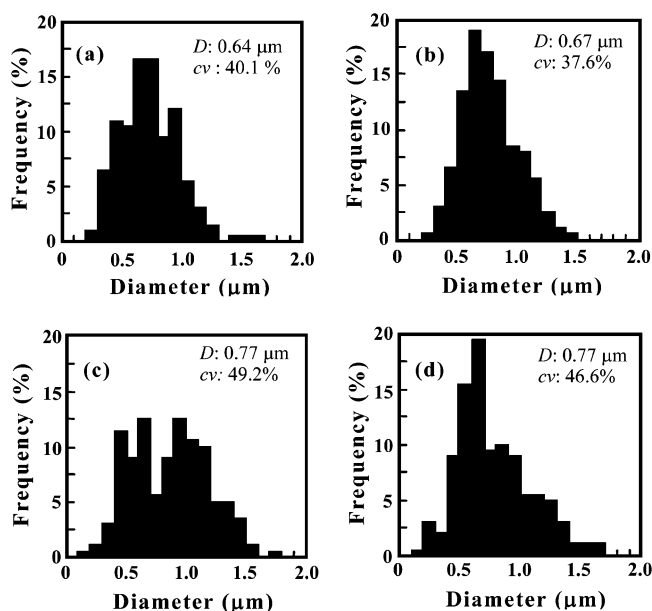


Figure 3. Diameter distribution diagrams of particles prepared at 240 °C for (a) 30 s, (b) 5 min, (c) 1 h, and (d) 6 h. *D* and *cv* denote an average diameter and a coefficient of variation, respectively.

particles were first investigated in the course of polymerization at *T_{ad}* of 240 °C. They are plotted in Figure 1a,b with the recovery yield of dissolved oligomers. The number of the particles (*N*) was calculated with the yield (*Y*), the average diameter (*D*), and the density (*ρ*) of 1.51–1.56 g cm⁻³ according to the following equation.

$$N = \frac{6Y}{\rho\pi D^3}$$

The yield of the particles increases rapidly within 5 min, and the recovery yield of the dissolved oligomers decreases correspondingly. The incipient precipitates were observed on a SEM, and they exhibit spherical morphology as shown in Figure 2a. This result reveals that the particles formed via liquid–liquid phase separation grow with the consecutive supply of the oligomers from solution phase. The diameter also increases rapidly with the yield. Interestingly, the number of the particles decreases significantly at the initial stage of the polymerization. Distribution diagrams of the diameter are shown in Figure 3. The distribution shifts toward longer diameter up to 1 h with exhibiting unimodality, and the values of the coefficient of variation (*cv*) were almost constant. These results indicate that the particles grew by not only the consecutive supply of oligomers but also the coalescence of droplets at the initial stage

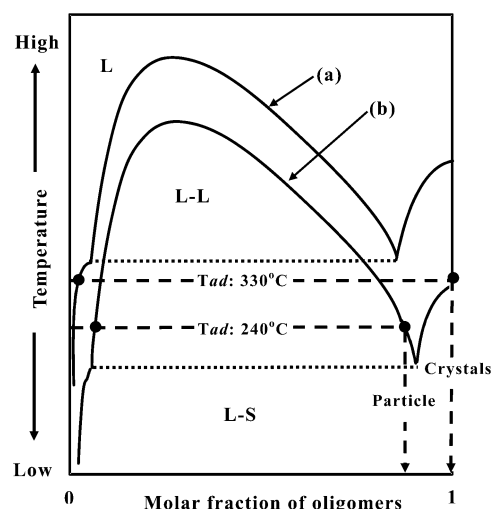


Figure 4. Schematic illustration of *C–T* diagrams for the system of TS10 and oligomers. Phase separation curves of a and b are for the oligomers prepared at *T_{ad}* of 240 and 330 °C, respectively. L: miscible liquid phase, L–L: two liquids phase, L–S: liquid and solid phase.

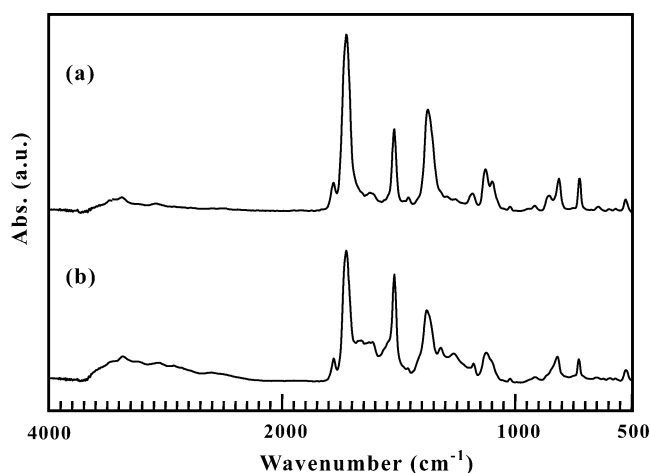


Figure 5. IR spectra of PPPI products obtained at (a) 330 °C and (b) 240 °C at the initial stage of polymerization.

of the polymerization. Even though Ostwald ripening process is not completely excluded from these results, the contribution of the ripening process is likely very few because further polymerization in the droplets reduces the solubility of the oligomers into the solvent due to the increase of molecular weight.

The changes in the yield of the crystals and the recovery yield of the dissolved oligomers prepared at *T_{ad}* of 330 °C were

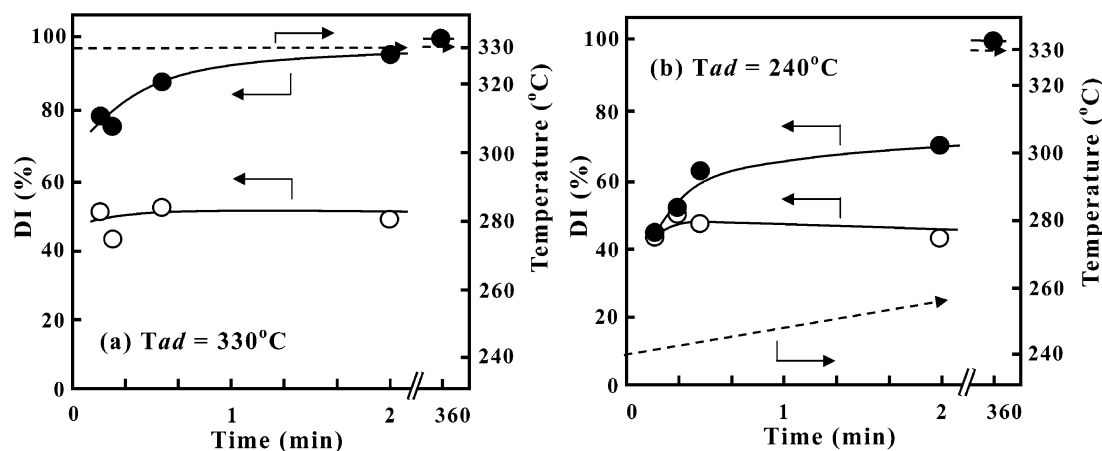


Figure 6. Plots of DI values of precipitates (●) and recovered oligomer (○) at (a) T_{ad} of 330°C and (b) 240°C as a function of polymerization time with temperature profile (dash line).

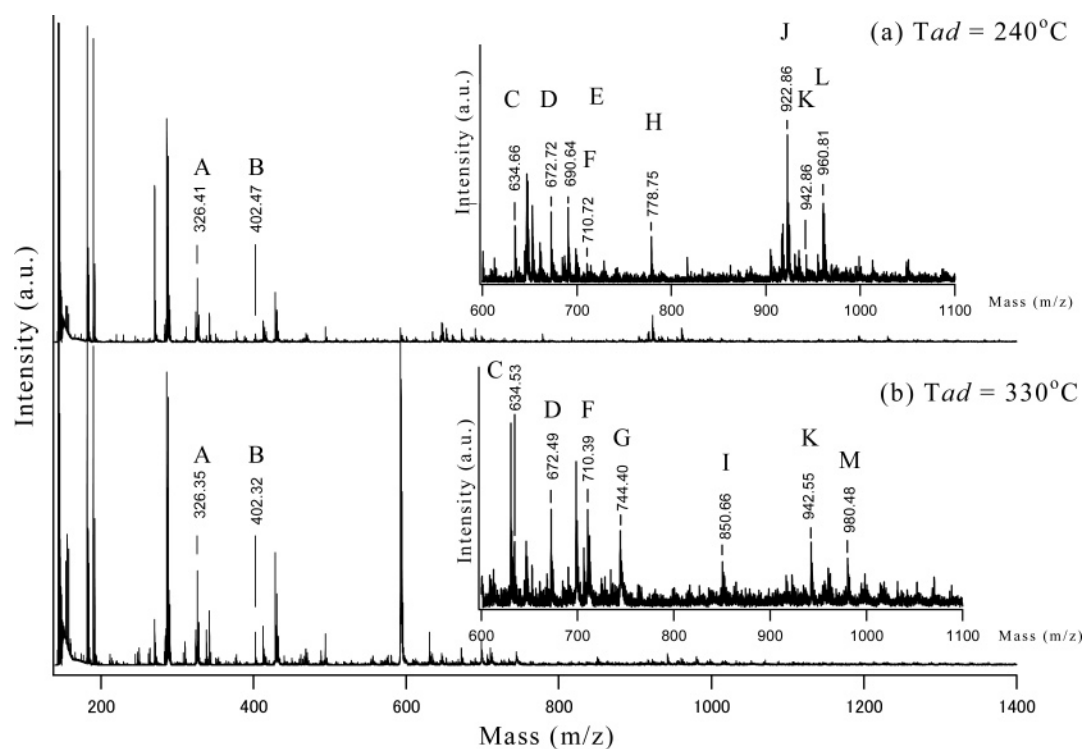
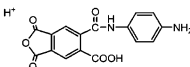
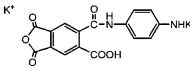
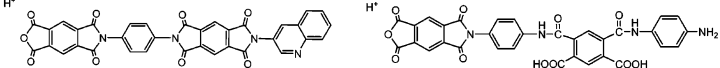
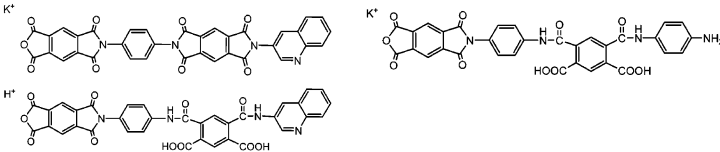
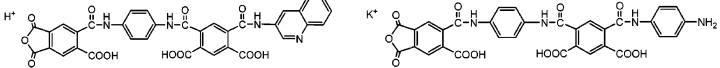
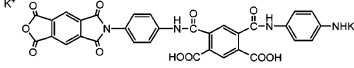
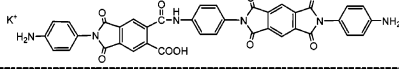
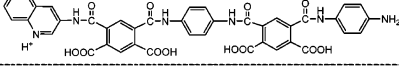
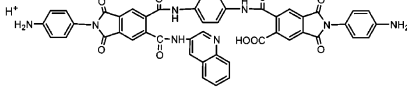
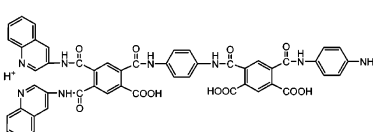
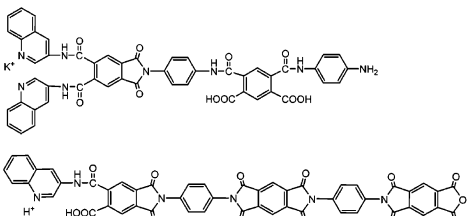
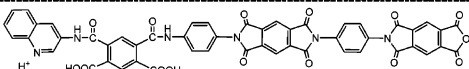
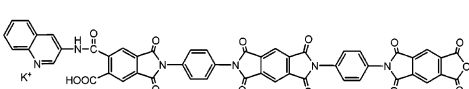


Figure 7. MALDI-TOF mass spectra of oligomers obtained from solution right after precipitation at (a) 240°C and (b) 330°C .

measured next in the course of the polymerization. They are also plotted in Figure 1c, and the morphology of the initial precipitates is shown in Figure 2b. The yield of the crystal increases rapidly, and the recovery yield of the dissolved oligomers decreases correspondingly with time. This result also reveals that the crystals grow with the consecutive supply of the oligomers as well as the particles. The products prepared for 30 s exhibits a clear crystal habit differing from the morphology of the incipient products of the particles. This morphological feature provides for unambiguous evidence of the crystallization. Reaction-induced phase separation of oligomers in poor solvent is describable on the analogous concentration–temperature phase diagram (C – T phase diagram) to that of partially miscible polymer–solvent system as schematically shown in Figure 4.^{16–18} The phase separation curve in the repulsive system can be written as the combination of the freezing point curve of the oligomers and the upper critical

solution temperature type dissolution curve. The oligomers are formed by the polymerization reaction, and the molecular weight of oligomers increases in the solution. The phase separation curve shifts toward higher temperature with increase of molecular weight of oligomers. When the molecular weight of oligomers exceeds critical value, the oligomers are in supersaturation state and then phase-separated. If the supersaturated oligomers cross the freezing point curve, they are precipitated by the crystallization to form the crystals, and the polymer crystals are finally formed by the postpolymerization in the crystals. On the other hand, if the dissolution curve is crossed, the oligomers are precipitated through liquid–liquid phase separation and the droplets of the dense phase are generated in the dilute phase. Finally polymer particles are formed due to the solidification of the droplets caused by the further polymerization in the droplets. The result that the higher temperature is favorable to induce the crystallization seems to be in conflict

Table 1. Structural Assignments of Peaks in the MALDI-TOF Mass Spectra Reported in Figure 7a and 7b

peak code	mass (m/z)			structure
	measured		calculated	
	(a)	(b)		
A	326.41	326.35	327.26	
B	402.49	402.32	403.46	
C	634.66	634.53	635.50	
D	672.72	672.49	673.60	
E	690.64	-	691.62	
F	710.72	710.39	711.70	
J	-	744.40	745.70	
H	778.75	-	779.68	
I	-	850.66	851.78	
J	922.86	-	923.86	
K	942.82	942.55	943.94 943.78	
L	960.81	-	961.76	
M	-	980.48	981.84	

with this phase-separation behaviors. Crystallization is usually induced at lower temperature, as explained on *C*–*T* phase diagram. Figure 5 shows IR spectra of the precipitates collected just after the phase separation. The spectra of the precipitates prepared at *Tad* of 240 and 330 °C were different, and the characteristic peaks of the amic acid moiety were seen in the spectrum at *Tad* of 240 °C. The relative intensity of imide C–N stretching at 1380 cm^{−1} to 1,4-phenylene C=C stretching at

1500 cm^{−1} is much larger at *Tad* of 330 °C than at *Tad* of 240 °C. To account for the difference in the chemical structure, the DI values of the precipitates and the recovered oligomers were estimated by quantifying the absorption intensity ratio between C=C stretching and C–N stretching. They were plotted as a function of polymerization time in Figure 6 with the polymerization temperature profiles. In the case of *Tad* of 240 °C, the DI value of the precipitates showed lower than 50% at the initial

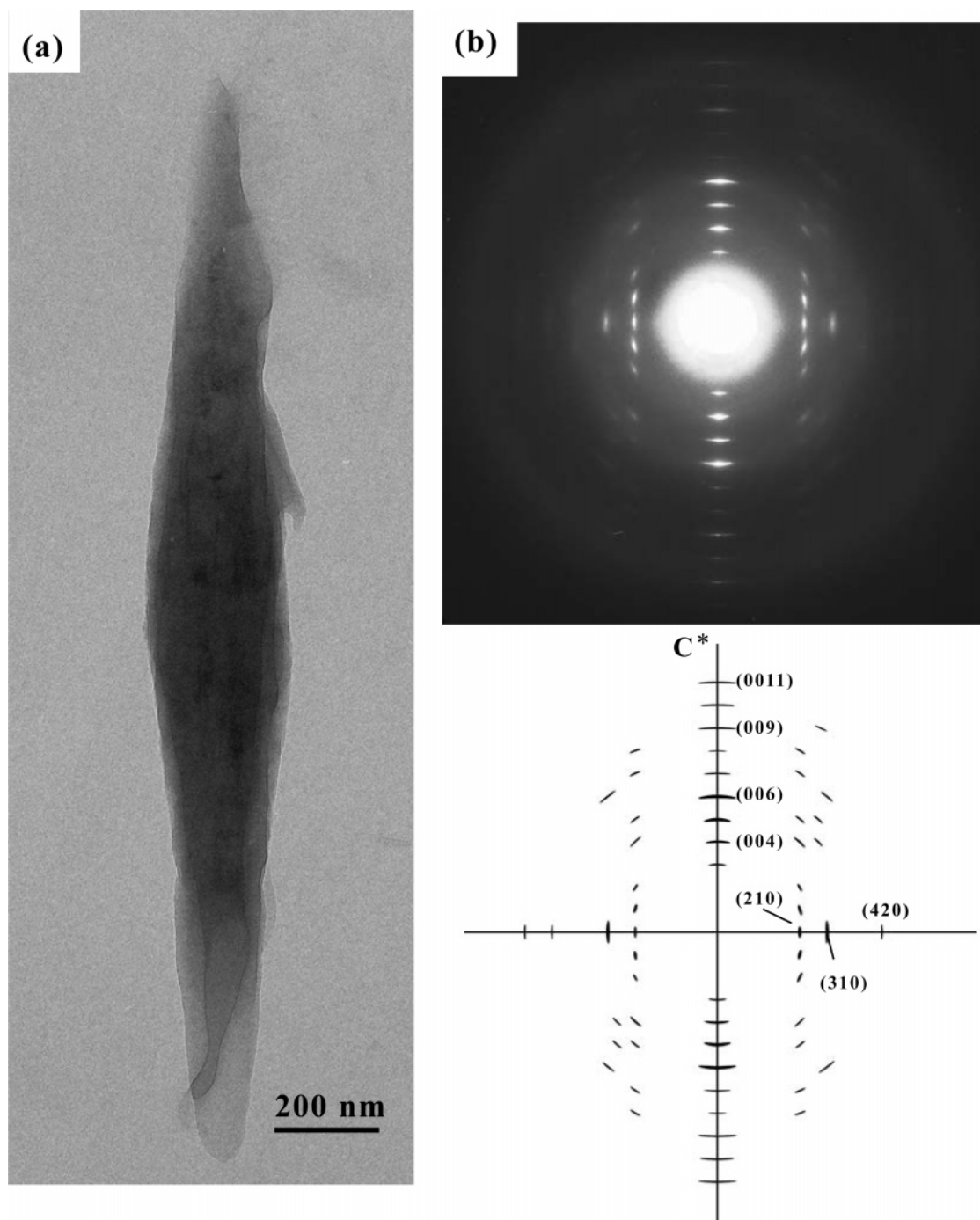


Figure 8. Transmission electron micrograph (a) and electron diffraction pattern (b) obtained from PPPI lozenge-shaped crystal by incident of electron beam perpendicular to plane of the crystal.

stage of the polymerization and then increased with time. This means that the oligomers rich in amic acid moiety are phase-separated. On the other hand, the DI value of the precipitates prepared at T_{ad} of 330 °C was higher than 70% from right after the phase separation and then also increased with time. The DI value of the recovered oligomers is constant at 50% in the course of the polymerization. These results reveal that the oligomers rich in imide moiety are phase-separated at 330 °C. Figure 7 shows the MALDI-TOF MS spectra of recovered oligomers at T_{ad} of 240 and 330 °C. The peaks in these spectra are identified in Table 1 according to the previous results.¹⁴ Both the oligomers prepared at 240 and 330 °C consist of imide and amic acid moieties. Four peaks at 690.6, 778.7, 922.9, and

960.8 are detected only in the spectrum of the oligomers prepared at T_{ad} of 240 °C, identified as the oligomers containing amic acid moiety. On the other hand, three peaks at 744.4, 850.7, and 980.5 are detected only in the spectrum of the oligomers prepared at T_{ad} of 330 °C, identified as the oligomers containing imide moiety. These results are identical with the discussion based on the results of the DI values, and the morphologies are quite susceptible to the DI value of the oligomers. The polymerization at the higher T_{ad} leads to the formation of oligomers rich in imide moiety in the solution and they are subsequently phase-separated. The freezing point curve of oligomers tends to shift toward higher temperature on C – T phase diagram with increasing the content of imide moiety due

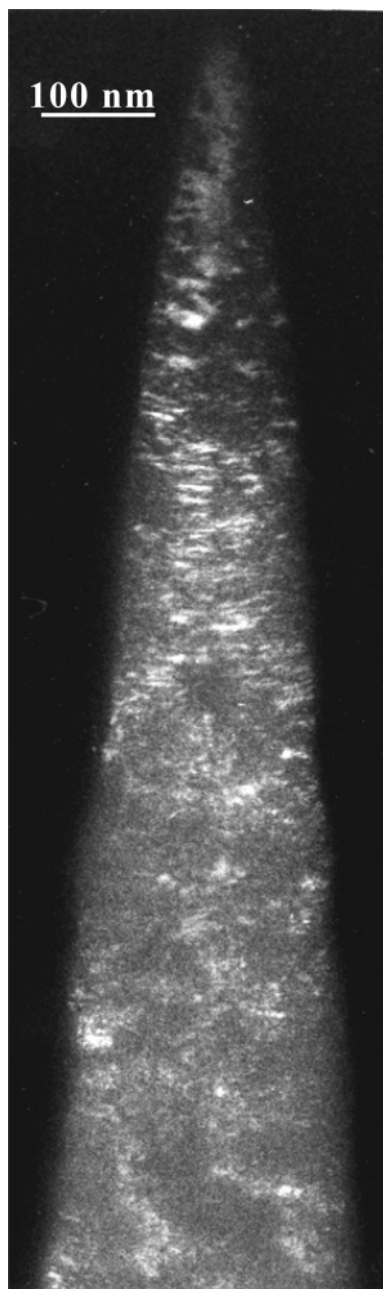


Figure 9. Dark field image of lozenge-shaped crystal taken by using the 110 and 200 reflections simultaneously.

to the entropic contribution caused by the increase of the rigidity. In contrast to this, the dissolution curve shifts toward lower temperature with increasing the content of imide moiety. These shifts bring about the expansion of the region of the liquid and solid phase, and therefore the oligomers are phase-separated by the crystallization. On the other hand, the oligomers containing much amic acid moiety have the lower freezing point curve due to the isomeric mixture of para and meta catenations in amic acid moiety, resulting in the expansion of two immiscible liquid phases. Therefore, the oligomers prepared at *Tad* of 240 °C tend to precipitate via the liquid–liquid-phase separation, leading to the formation of the particles. Additionally, both the structural irregularity caused by the para and meta catenations and the formation of the intermolecular hydrogen bonding through amide linkage and carboxyl group in amic acid moiety lowers the crystallizability of the oligomers, preventing the formation of the crystals.

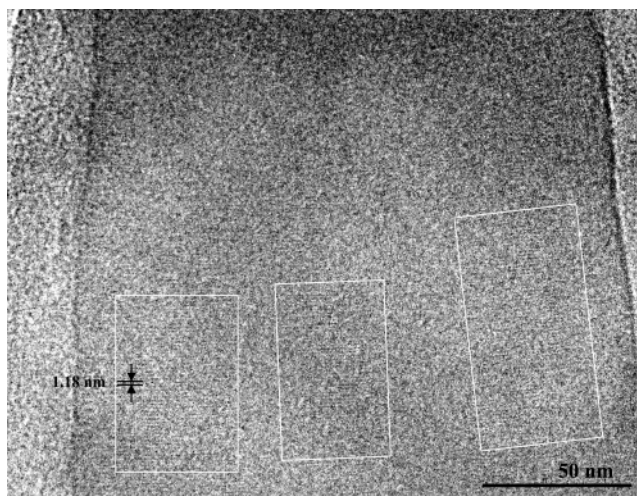


Figure 10. High-resolution image of a lozenge-shaped crystal.

3.2. Structure of Lozenge-Shaped Crystals. The lozenge-shaped crystal was observed on a TEM to analyze the structure. Figure 8 shows a transmission electron micrograph and a selected area electron diffraction pattern. The crystal has contrast from center to tip, and the stratified contrasts could be observed at the tip part of the crystal. The lozenge-shaped crystals are composed of the stacking layer structure. The diffraction pattern was not a true fiber pattern of cylindrical symmetry and many sharp spots are observed from lower to higher diffractions. These spots can be indexed with the PPPI orthorhombic unit cell,^{7,19} and the meridian of the pattern is corresponding to *c* axis of the crystal. This result indicates that the polymer molecules are aligned along the long axis of the lozenge-shape crystals. The spots on the meridian are diffuse. This broadening seems to be due to orientational fluctuation of crystallites, the axial shifted polymer molecules structure,^{20–22} or the crystal size effects.²³ Since, the broadening of other spots is not observed, this broadening indicates the orientational fluctuation of crystallites.

A dark field electron micrograph of the lozenge-shaped crystals was taken by using 110 and 200 reflections simultaneously as shown in Figure 9. The crystal is not uniformly bright. The fine bright striations oriented in the horizontal direction are observed in many places. The average width and average length of the bright striations were measured to be about 28 and 47 nm, respectively. This fact suggests that some regions of internal distortions are present with in the crystal. As aforesaid, the crystals are formed by the rapid precipitation of oligomers and this rapid growth might result in the internal distortions.

A high-resolution bright field electron micrograph of the lozenge-shape crystal was taken as shown in Figure 10. From the micrograph, lattice fringes can be distinguished running perpendicular to the long axis of the crystal. PPPI molecules are oriented perpendicular to the fringe direction. The spacing of the lattice fringes was measured directly from the image to be 1.18 nm, which corresponds to the interplanar spacing of (001) planes. The high contrast and extended lateral size of the (001) fringes are remarkable and provide for unambiguous evidence of the regularity of the axial registry between neighboring molecules on the PPPI crystal.

4. Conclusions

PPPI crystals such as lozenge-shaped crystal and starlike aggregates of needlelike crystals were obtained at *Tad* of 280 and 330 °C. On the contrary, only the particles were obtained

at *Tad* of 240 °C. The oligomers containing many imide moieties, which were generated in solution at higher temperature, crystallized to form the polymer crystal. On the other hand, the oligomers rich in amic acid moiety, which were generated in solution at lower temperature, precipitated through liquid–liquid phase separation and then formed the particles. The addition temperature of PPDA considerably influenced the morphology of PPPI. The obtained lozenge-shaped crystal showed excellent crystallinity, and the molecular chains were oriented along the long axis of the crystal with slight distortion.

References and Notes

- (1) Rauter, H.; Matyushin, V.; Alguet, Y.; Pittner, F.; Schalkhammer, T. *Macromol. Symp.* **2004**, *217*, 109.
- (2) Woodson, M.; Liu, J. *J. Am. Chem. Soc.* **2006**, *128*, 3760.
- (3) Sumpter, B. G.; Noid, D. W.; Barnes, M. D.; Otaigbe, J. U. *Encyclopedia. Nanosci. Nanotechnol.* **2004**, *8*, 873.
- (4) Caseri, W. *Chem. Nanostruct. Mater.* **2003**, 359.
- (5) For examples: Mattsen, M. W.; Schick, M. *Cur. Opin. Colloid Int. Sci.* **1996**, *1*, 329. Zhang, S.; Altman, M. *React. Funct. Polym.* **1999**, *41*, 91. Collier, J. H.; Messersmith, P. B. *Adv. Mater.* **2004**, *16*, 907. Leibler, L. *Prog. Polym. Sci.* **2005**, *30*, 898. Shimizu, T.; Masuda, M.; Minamikawa, H. *Chem. Rev.* **2005**, *105*, 1401.
- (6) For examples: Baumgarten, P. K. *J. Colloid Interface Sci.* **1971**, *36*, 71. Megelski, S.; Stephens, J. S.; Chase, D. B.; Rabolt, J. F. *Macromolecules* **2002**, *35*, 8456.
- (7) For examples; Cassidy, P. E. *Thermally Stable Polymers, Syntheses and Properties*; Marcel Dekker Inc.: New York, 1980. Blumstein, A. *Liquid Crystalline Order in Polymers*; Academic Press: London, 1978. Seymour, R. B.; Kirshenbaum, G. S. *High Performance Polymers; Their Origin and Development*; Elsevier: New York, 1986.
- (8) Tashiro, K.; Kobayashi, M. *Sen-i Gakkaishi* **1987**, *43*, 78.
- (9) Sroog, C. E. *J. Polym. Sci., Macromol. Rev.* **1976**, *11*, 161.
- (10) Bessonov, M. I.; Koton, M. M.; Kudryavtsev, V. V.; Laius, L. A. *Polyimides: Thermally Stable Polymers*; Consultants Bureau: New York, **1987**.
- (11) Wilson, D.; Stenzenberger, H. D.; Hergenrother, P. M. *Polyimides*; Blackie: New York, 1990.
- (12) Mittal, K. L. *Polyimides, Synthesis, Characterization, and Application*; Plenum Press: New York, 1984.
- (13) Kimura, K.; Zhuang, J.-H.; Wakabayashi, K.; Yamashita, Y. *Macromolecules* **2003**, *36*, 6292.
- (14) Gies, A. P.; Nonidez, W. K.; Anthamatten, M.; Cook, R. C.; Mays, J. W. *Rapid Commun. Mass Spectrosc.* **2002**, *16*, 1903.
- (15) Lee, H. J.; Won, J.; Park, H. C.; Lee, H.; Kang, Y. S. *J. Membr. Sci.* **2000**, *178*, 35.
- (16) Kimura, K.; Inoue, H.; Kohama, S.; Yamashita, Y.; Sakaguchi, Y. *Macromolecules* **2003**, *36*, 7721.
- (17) Richards, R. B. *Trans. Faraday Soc.* **1946**, *42*, 10.
- (18) Flory, P. J.; Mandelkern, L.; Hall, H. K. *J. Am. Chem. Soc.* **1951**, *73*, 2532.
- (19) Baklagina, Y. G.; Milevskaya, I. S.; Yefanova, N. V.; Sidorovich, A. V.; Zubkov, V. A. *Vysokomol. Soyed.* **1976**, *A18*, 1235.
- (20) Shimamura, K.; Minter, J. R.; Thomas, E. L. *J. Mater. Sci. Lett.* **1983**, *2*, 54.
- (21) Adams, W. W.; Kumar, S.; Martin, D. C.; Shimamura, K. *Polym. Commun.* **1989**, *30*, 285.
- (22) Shimamura, K.; Uchida, T. *J. Macromol. Sci. Phys.* **2000**, *B39*, 667.
- (23) Peterlin, A.; Sakaoku, K. *Macromol. Chem.* **1967**, *108*, 234.

MA062032Y